Box-size dependence and breaking of translational invariance in the velocity statistics computed from three-dimensional turbulent Kolmogorov flows

I. E. Sarris, H. Jeanmart, D. Carati, and G. Winckelmans

Citation: Physics of Fluids (1994-present) **19**, 095101 (2007); doi: 10.1063/1.2760280
View online: http://dx.doi.org/10.1063/1.2760280
View Table of Contents: http://scitation.aip.org/content/aip/journal/pof2/19/9?ver=pdfcov
Published by the AIP Publishing

Box-size dependence and breaking of translational invariance in the velocity statistics computed from three-dimensional turbulent Kolmogorov flows

I. E. Sarris[a)]
Statistical and Plasma Physics, CP 231, Campus Plaine, Université Libre de Bruxelles, 1050 Bruxelles, Belgium

H. Jeanmart[b)]
Department of Mechanical Engineering, Université catholique de Louvain, 1348 Louvain-la-Neuve, Belgium

D. Carati[c)]
Statistical and Plasma Physics, CP 231, Campus Plaine, Université Libre de Bruxelles, 1050 Bruxelles, Belgium

G. Winckelmans[d)]
Department of Mechanical Engineering, Université catholique de Louvain, 1348 Louvain-la-Neuve, Belgium

(Received 23 March 2007; accepted 21 June 2007; published online 5 September 2007)

The Kolmogorov flow generated by a stationary one-dimensional forcing varying sinusoidally in space is studied using direct numerical simulations with periodic boundary conditions. The velocity statistics are considered for various computational domains ranging from the minimal cubic box with size equal to the forcing wavelength to significantly larger domains. For the minimal computational domain, the velocity statistics exhibit symmetries that are directly imposed by the forcing properties. However, for larger domains, the translational invariance in the streamwise direction appears to be broken and the turbulence statistics depend on the computational box aspect ratio. © *2007 American Institute of Physics*. [DOI: 10.1063/1.2760280]

I. INTRODUCTION

The Kolmogorov flow is generated by a stationary forcing which varies sinusoidally in space. As shown in Fig. 1, the forcing is assumed to be aligned with the x axis and is modulated along the y axis:

$$F_x = A \sin(k_f y), \quad F_y = F_z = 0. \tag{1}$$

This problem is rather academic since generating such a periodic forcing in an unbounded flow is difficult to achieve in a real experiment. Nevertheless, it allows for a fairly detailed analytical treatment. For instance, several studies concerning the stability, transition, and turbulence of the flow have been published[1–6] for two-dimensional domains. As expected, for large forcing amplitudes A or for small viscosities, the flow generated by the force (1) becomes unstable. In addition, the simplicity of the Kolmogorov flow makes it a good test case for investigating three-dimensional turbulence in a situation that is simultaneously inhomogeneous, sheared, and anisotropic. For instance, it has been used for studying the drag reduction in viscoelastic fluid models of dilute polymer solutions under large scale forcing.[7] In addition, being periodic in the three directions, the Kolmogorov flow can be computed using spectral codes and quite large Reynolds numbers are achievable numerically. Fairly large direct numerical simulations (DNS)[8] have already been produced for this flow which might also qualify as an interesting test case for assessing subgrid scale model in large-eddy simulations (LES). Woodruff *et al.*[9] have studied the dependence of grid size for a large-eddy simulation experiment of the turbulent Kolmogorov flow, while the performance of various LES models for this flow was reported in Ref. 10. Despite its periodicity, this flow is more complex and thus more challenging than the classical isotropic turbulence test case that has been used intensively in LES validations. In particular, as discussed in Sec. II, both the mean velocity and the average fluctuations of velocity (Reynolds stresses) depend explicitly on y.

In most of the existing literature, the Kolmogorov flow has been considered in a cubic box. However, the present study shows that the complexity of the Kolmogorov flow goes much further than the expected y inhomogeneity of the turbulence statistics. Indeed, in a series of runs presented in Sec. III, it appears that the Reynolds number is not the unique parameter characterizing the Kolmogorov flow. The aspect ratio of the computational box is shown in Sec. IV to also play an important role, making the statistics of the flow more dependent on the computational box size than expected. In Sec. V, breaking of the translational invariance are observed when strongly elongated computational boxes are considered. In particular, the type of forcing suggests that the time averaged velocity is aligned with the forcing. However, a nonzero velocity perpendicular to the force is also observed under certain conditions. Moreover, complex structures are observed in the turbulence fields in some cases. These properties are reminiscent of two-dimensional results obtained previously.[6]

[a)]Electronic mail: isarris@ulb.ac.be
[b)]Electronic mail: jeanmart@term.ucl.ac.be
[c)]Electronic mail: dcarati@ulb.ac.be
[d)]Electronic mail: winckelmans@term.ucl.ac.be

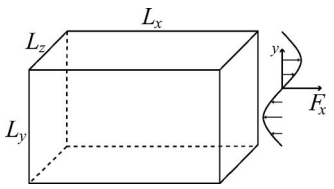

FIG. 1. Computational box for the Kolmogorov flow.

II. AVERAGED PROPERTIES OF THE KOLMOGOROV FLOW

The velocity field u_i is assumed to be described by the incompressible Navier-Stokes equations:

$$\partial_t u_i + \partial_j(u_i u_j) = -\partial_i p + \nu\nabla^2 u_i + F_i, \tag{2}$$

where the pressure (divided by the density) p is determined by the incompressibility condition $\partial_i u_i = 0$ and the forcing term is given by (1). The range of parameters that are considered in the present study corresponds to high enough Reynolds numbers so that a fully turbulent regime can be expected. In particular, the purpose of this work is not to investigate the cascade of instabilities that leads to the turbulent regime in the Kolmogorov flow. The statistics are collected when the flow appears to be fully developed and when global quantities such as energy and dissipation seem to be statistically stationary. In practice, this is achieved by computing these statistics without taking into account a possible transient period influenced by the initial conditions which are given by three-dimensional random velocity fields.

The simulation are performed using a fully dealiased spectral code.[13] The flow is thus considered in a periodic rectangular box of size $L_x \times L_y \times L_z$. In the following section, the influence of the aspect ratios on the flow statistics will be explicitly considered. The aspect ratios are defined as the ratios between the computational sizes and the forcing periodicity length $L_f = 2\pi/k_f$:

$$r_x = \frac{L_x}{L_f}, \quad r_y = \frac{L_y}{L_f}, \quad r_z = \frac{L_z}{L_f}. \tag{3}$$

In many branches of computational fluid dynamics, the aspect ratios are obtained by comparing the length scales of the physical domain. However, we are in a special case since our simulations are supposed to represent an unbounded flow. In homogeneous turbulence, the domain size is usually chosen to ensure that the velocity statistics are independent of the ratio between the computational box size and the integral scale. However, in the Kolmogorov flow, the forcing length L_f is an intrinsic length scale and it is natural to explore the possible dependence of the numerical results on the ratios r_x, r_y, and r_z.

Traditionally, the description of a turbulent flow is limited to the lowest moments of the velocity field [$\langle u_i\rangle$, $\langle u_i u_j\rangle$, $\langle(\partial_k u_i)(\partial_l u_j)\rangle$, etc.]. Several definitions of the average will be used for describing the Kolmogorov flow. Time average is the most natural since the external constraints (geometry and forcing) are time independent. The statistics of the flow are thus expected to be stationary. Moreover, in order to increase the convergence of the statistics, it is usual to make an additional averaging over the plane of symmetry (z-x). It will be shown however that, depending on the value of the aspect ratios (3), the flow is not statistically homogeneous in the x direction. In that case, the average over t and over t and x may differ, and it is thus important to specify the variable(s) on which the average is taken. For instance, the operator $\langle\cdots\rangle_t$ refers to the time averaging, while the operator $\langle\cdots\rangle_{t,x,z}$ stands for averaging over time and over x and z. In the present numerical experiments, the time-averaged properties of the flow appear to be independent of the transverse coordinated z. For this reason, the average $\langle\cdots\rangle_t$ is systematically replaced by the average $\langle\cdots\rangle_{t,z}$, which provides the same information but converges much more rapidly. In particular, the following quantities have been studied:

$$U_i = \langle u_i\rangle_{t,z}, \tag{4}$$

$$M_{ij} = \langle u_i u_j\rangle_{t,z} - \langle u_i\rangle_{t,z}\langle u_j\rangle_{t,z}, \tag{5}$$

$$\mathcal{P} = \langle p\rangle_{t,z}. \tag{6}$$

Relations between these first- and second-order moments are directly obtained by applying the $\langle\cdots\rangle_{t,z}$ operator to the Navier-Stokes equations:

$$\tilde{\nabla}_j M_{ij} + U_j\tilde{\nabla}_j U_i = -\tilde{\nabla}_i\mathcal{P} + \nu\tilde{\nabla}^2 U_i + F_i, \tag{7}$$

where $\tilde{\nabla} = (\partial_x, \partial_y, 0)$. The corresponding continuity equation $\tilde{\nabla}_i U_i = 0$ thus reads:

$$\partial_x U_x + \partial_y U_y = 0. \tag{8}$$

Although these relations are much simpler than the original Navier-Stokes equations, they remain fairly complicated to analyze. Moreover, for low aspect ratios ($r_x = r_y = r_z = 1$), the statistics of the flow appear to be independent on the x coordinate. For that reason, the following quantities, obtained by using the operator $\langle\cdots\rangle_{t,z-x} = \langle\langle\cdots\rangle_{t,z}\rangle_x$, have often been reported in the literature:

$$V_i = \langle u_i\rangle_{t,z-x} = \langle U_i\rangle_x, \tag{9}$$

$$R_{ij} = \langle u_i u_j\rangle_{t,z-x} - \langle u_i\rangle_{t,z-x}\langle u_j\rangle_{t,z-x} = \langle M_{ij}\rangle_x + Z_{ij}, \tag{10}$$

$$P = \langle p\rangle_{t,z-x} = \langle\mathcal{P}\rangle_x, \tag{11}$$

where $Z_{ij} = \langle U_i U_j\rangle_x - \langle U_i\rangle_x\langle U_j\rangle_x$ is a function of the average velocity U_i. Relations for these quantities are also readily obtained by averaging over x the equations for M_{ij} and U_i:

$$0 = F_x - \partial_y R_{xy} + \nu\partial_y^2 V_x, \tag{12}$$

$$0 = -\partial_y P - \partial_y R_{yy}, \tag{13}$$

$$0 = -\partial_y R_{yz} + \nu\partial_y^2 V_z, \tag{14}$$

while the continuity equation reduces to

$$\partial_y V_y = 0. \tag{15}$$

It is shown in the next sections that V_i and R_{ij} depend quite strongly on the aspect ratio r_x. Moreover, the translational invariance is clearly broken in the Kolmogorov flow, characterized by statistically significant differences between R_{ij} and

TABLE I. Characteristics of the runs in the sets A and B.

	n_x/r_x	n_y/r_y	n_z/r_z	$\nu\tau_\star/l_\star^2$
Set A	128	128	128	0.007
Set B	256	256	256	0.0028

M_{ij} or between U_i and V_i, for $r_x \geq 2$. Some interesting information can however be derived from these equations. First, the average continuity, i.e., Eq. (15), implies that V_y is independent of y. Thus, by conservation of momentum, if the initial conditions correspond to zero total momentum in the y direction, we have $V_y=0$.

Equation (13) is automatically satisfied when the pressure is derived from the incompressibility condition. It implies that the mean pressure is also a function of y. Equation (14) implies that $R_{yz}-\nu\partial_y V_z$ is independent of y and, since $V_z=0$, that R_{yz} is independent of y. The invariance of the force under reflection $\mathbf{1}_z \rightarrow -\mathbf{1}_z$ and the symmetry of the computational domain could lead to the conclusion that R_{yz} should vanish. However, as a consequence of the translational invariance breaking in the Kolmogorov flow for large aspect ratio r_x, this component of the Reynolds stress is observed to remain different from zero. Finally, Eq. (12) is interesting since it can be used to check the stationarity of the flow. Integrating this relation in y leads to the following balance between three terms (that can be evaluated separately):

$$R_{xy}(y) = \nu\partial_y V_x(y) - \frac{A}{k_f}\cos(k_f y). \tag{16}$$

III. DIRECT NUMERICAL SIMULATION

Before discussing the details of the DNS that have been performed, it is worth introducing the characteristic length scale, velocity scale, and time scale of the Kolmogorov flow. The characteristic length scale of the flow is imposed by the forcing: $l_\star=k_f^{-1}$. In the laminar regime, the forcing generates a unidirectional flow parallel to the x axis, $u_x=A/(\nu k_f^2)\sin(k_f y)$. The characteristic laminar velocity is thus $U=A/(\nu k_f^2)$. However, in the turbulent regime, the characteristic velocity is not supposed to depend on the viscosity and should depend only on the forcing amplitude A and on k_f. The dimensional analysis thus leads to $v_\star=A^{1/2}k_f^{-1/2}$. Finally, the characteristic time scale is defined by $\tau_\star=l_\star/v_\star=(Ak_f)^{-1/2}$. The Reynolds number based on $l_\star$ and $v_\star$ is thus given by:

$$\mathrm{Re} = \frac{A^{1/2}}{k_f^{3/2}\nu}. \tag{17}$$

This number is related to the Grashof number $\mathrm{Gr}=\mathrm{Re}^2$ also used to characterize forced flows.[12] Direct numerical simulations of the Kolmogorov flow have been achieved using a pseudo-spectral code with different resolutions and various box sizes. We present two sets of runs (sets A and B) corresponding to different viscosities and grid sizes, the parameters of which are summarized in Table I (in each case, the following numerical values have been used during the computation: $A=1$ and $k_f=1$; thus $L_f=2\pi$ and $l_\star=v_\star=\tau_\star=1$).

For all runs in the set A, the viscosity and thus the Reynolds number defined by (17) is the same and the computational mesh sizes $\Delta_x=L_x/n_x$, $\Delta_y=L_y/n_y$, $\Delta_z=L_z/n_z$ are identical and correspond to 128 mesh points per length L_f. Hence, the numbers of grid points in each direction divided by the aspect ration are identical ($n_x/r_x=n_y/r_y=n_z/r_z=128$). Runs with aspect ratio r_x up to 8 have been performed, corresponding to simulations with up to $1024\times128\times128$ grid points. All runs in the set B are also characterized by the same viscosity, lower than in set A, and correspond to a larger Reynolds number. They have been performed using a larger number (256) of mesh points per length L_f in order to ensure that the flow is well resolved. Runs with up to $1024\times256\times256$ grid points have been performed. They have been used for investigating the Reynolds number dependence of the Kolmogorov flow statistics (see Sec. IV).

The code is fully de-aliased and the time-stepping is based on a third-order Runge-Kutta procedure for the nonlinear and forcing terms. The viscous term is integrated through an analytic factor. Stability is obtained by adapting the time step according to the condition $\delta t < C\Delta/v_{\max}$. The grid size is given by $\Delta=\min(\Delta_x,\Delta_y,\Delta_z)$, and $v_{\max}$ is the maximal velocity. The parameter C has to be chosen low enough to ensure the stability of the convective nonlinear term. Values of C of the order of unity are known to ensure stability. Accuracy of the integration scheme is however significantly improved when using $C=0.5$. The molecular viscosity has been chosen to ensure that the product of the largest wavevector K and the dissipation length $\eta=(\nu^3/\epsilon)^{1/4}$ is of the order of 1.5. In order to make easier the comparison with DNS of isotropic turbulence, we also provide in Table II the microscale Reynolds number, defined as $\mathrm{Re}_\lambda=u'\lambda/\nu$, where

$$u' = \sqrt{\frac{2E'}{3}}, \tag{18}$$

$$\lambda = \sqrt{\frac{15\nu u'^2}{\epsilon}}. \tag{19}$$

The turbulent kinetic energy is defined by

$$E' = \frac{1}{2L_yL_x}\int_0^{L_x}\int_0^{L_y} dxdy \sum_i \left(\langle u_i^2\rangle_{t,z} - \langle u_i\rangle_{t,z}^2\right)$$
$$= \frac{1}{2L_yL_x}\int_0^{L_x}\int_0^{L_y} dxdy \sum_i M_{ii}, \tag{20}$$

and appears as the difference between the total energy E and the energy carried on by the averaged flow U_i. The dissipation ϵ can be computed indifferently from the total or the fluctuating velocity field since the average field is dominated by low k modes and, consequently, does not contribute significantly to the total dissipation.

The total integration time T is chosen to ensure that the statistics are reasonably converged. The convergence has been checked using two criteria. First, the right-hand side and the left-hand side of the relation (16) have been compared:

TABLE II. Characteristics of the DNS runs.

	r_x	r_y	r_z	R_λ	$\epsilon\tau_\star/v_\star^2$	$E/v_\star^2$	$E'/v_\star^2$	$K\eta$
A01	1	1	1	69.3	1.34	4.43	2.60	1.44
A01β	1	2	1	65.5	1.42	4.53	2.53	1.42
A01γ	1	3	1	66.1	1.43	4.64	2.56	1.41
A01δ	1	4	1	64.8	1.38	4.43	2.47	1.43
A01ϵ	1	6	1	62.8	1.41	4.58	2.42	1.41
A02	2	1	1	108.0	0.51	2.80	2.50	1.84
A03a	3	1	1	82.7	0.33	2.44	1.54	2.04
A03b	3	1	2	179.0	0.31	3.37	3.23	2.16
A03c	3	1	3	174.0	0.25	2.17	2.82	2.86
A03β	3	2	1	94.0	0.33	2.63	1.75	1.34
A04	4	1	1	78.9	0.27	2.30	1.33	2.12
A04β	4	2	1	90.3	0.43	3.26	1.92	1.51
A06	6	1	1	101.9	0.19	2.51	1.44	2.01
A08	8	1	1	101.8	0.16	2.58	1.32	1.95
B01	1	1	1	91.8	1.44	4.78	2.71	1.43
B02	2	1	1	118.1	0.61	2.84	1.89	1.78
B04	4	1	1	103.1	0.51	2.64	1.51	1.85

$$\gamma_1 = \frac{\int_0^{L_y} dy \left(R_{xy}(y) - \nu \partial_y V_x(y) + \frac{A}{k_f} \cos(k_f y) \right)^2}{\int_0^{L_y} dy R_{xy}^2(y)}. \quad (21)$$

Second, the mean energy injection ϵ_i due to the forcing has been compared to the total dissipation ϵ. For well converged statistics, these two quantities are expected to be equal, and we thus have computed the parameter:

$$\gamma_2 = \frac{(\epsilon_i - \epsilon)^2}{\epsilon^2}. \quad (22)$$

The energy injection rate can be computed as follows:

$$\epsilon_i = \frac{1}{L_y} \int_0^{L_y} V_x(y) F_x(y) dy. \quad (23)$$

The analytical form of the forcing being known, this relation can be integrated by part and leads to

$$\epsilon_i = \frac{A}{L_y k_f} \int_0^{L_y} dy \partial_y V_x(y) \cos(k_f y). \quad (24)$$

The quantity $\partial_y V_x(y)$ can be extracted from the balance equation (16), so that the energy injected into the system by the forcing is the sum of two terms:

$$\epsilon_i = \frac{A^2}{2\nu k_f} + \frac{A}{L_y \nu k_f} \int_0^{L_y} dy R_{xy}(y) \cos(k_f y). \quad (25)$$

The first term corresponds to the laminar case. The second is negative and shows the decrease of the forcing efficiency due to turbulence generation. Parameters γ_1 and γ_2 are reported in Table III. It must be acknowledged, however, that, even if measuring small values γ_1 and γ_2 is a necessary condition to have converged statistics, it may be not a sufficient condition.

IV. BOX-SIZE DEPENDENCE OF THE KOLMOGOROV FLOW

In previous studies of the Kolmogorov flow, the computational domain has been chosen to be cubic[8,11] with a linear size equal to the length of periodicity of the forcing. With the choice $k_f=1$, this amounts to imposing $L_x=L_y=L_z=L_f$.

TABLE III. The stationarity of the DNS is checked through the parameters γ_1 and γ_2 which are supposed to vanish for perfectly converged simulations.

	$T/\tau_\star$	γ_1	γ_2
A01	1589	1.2×10^{-4}	4.0×10^{-5}
A01β	350	8.3×10^{-4}	9.7×10^{-5}
A01γ	330	1.8×10^{-3}	9.5×10^{-5}
A01δ	250	2.4×10^{-3}	1.9×10^{-4}
A01ϵ	230	1.9×10^{-3}	1.6×10^{-4}
A02	1504	8.4×10^{-5}	3.4×10^{-6}
A03a	983	1.0×10^{-5}	3.5×10^{-6}
A03b	528	7.0×10^{-4}	1.1×10^{-5}
A03c	516	1.1×10^{-4}	1.8×10^{-5}
A03β	509	3.8×10^{-5}	5.4×10^{-6}
A04	701	8.6×10^{-6}	1.4×10^{-6}
A04β	528	1.8×10^{-4}	6.1×10^{-5}
A06	551	6.1×10^{-5}	4.0×10^{-6}
A08	519	2.9×10^{-5}	1.2×10^{-6}
B01	313	2.4×10^{-4}	8.4×10^{-5}
B02	309	1.1×10^{-3}	8.2×10^{-5}
B04	306	3.4×10^{-4}	5.4×10^{-5}

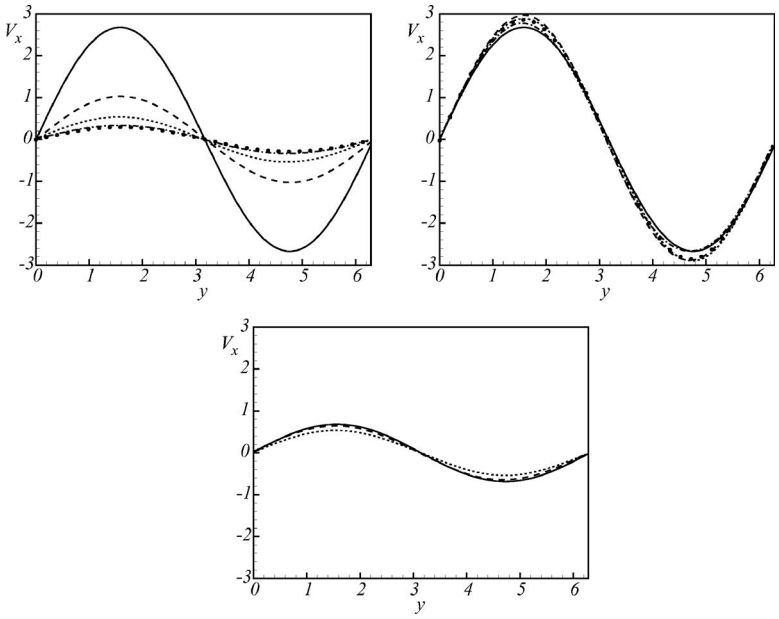

FIG. 2. Mean longitudinal velocity averaged over t and z-x for different r_x with $r_y=r_z=1$ (top left): A01 ($r_x=1$, solid); A02 ($r_x=2$, dash); A04 ($r_x=4$, dot); A06 ($r_x=6$, chained-dot); and A08 ($r_x=8$, circle). Same comparison for different r_y with $r_x=r_z=1$ (top-right): A01 ($r_y=1$, solid); A01β ($r_y=2$, dash); A01γ ($r_y=3$, dot); A01δ ($r_y=4$, chained-dot); and A01ϵ ($r_y=6$, circle). The figures corresponding to different r_y are presented for the same range of y for easier comparison. A similar comparison for different r_z is also shown for $r_x=3$ and $r_y=1$ (bottom): A03a ($r_z=1$, solid); A03b ($r_z=2$, dash); and A03c ($r_z=3$, dot).

However, nothing guarantees in the Kolmogorov flow that the characteristic length scales of the flow in the three directions will be significantly smaller than the domain sizes. In order to check this property, we introduce the following length scales:

$$\ell_i = \frac{\langle M_{ii}^{3/2} \rangle_{x\text{-}y}}{\epsilon}. \tag{26}$$

In the z direction, where no averaged motion is expected, the computational domain should not influence strongly the results. Most of the runs from the series B are characterized by $\ell_z \approx 1.4$, while runs in series A have $\ell_z \geq 1.5$. The largest ℓ_z is observed for run A08 ($\ell_z \approx 2.1$). Hence, in the worse case, the choice $L_z=L_f$ ensures that $L_z \approx 3\ell_z$, while typically L_z is between three and six times larger than ℓ_z. For this reason, we have mainly considered domains with $L_z=2\pi$. Exceptions are runs A03b-c, where $L_z=2L_f$ and $L_z=3L_f$ have been explored. Imposing the same periodicity in the y direction as for the forcing seems, of course, very natural ($r_y=1$). This is the choice adopted in almost all the runs from series A and B. It should be noted, however, that ℓ_y is not always much smaller than L_f. For this reason, we have also explored cases with higher r_y: A01β, A03β, and A04β ($r_y=2$) A01γ ($r_y=3$), A01δ ($r_y=4$), and A01ϵ ($r_y=6$).

Considering the simplicity of the forcing, one could assume that several mean flow statistics reported in Table II may have similar values, whatever the domain size. However, looking at Table II, one can readily see that this simple assumption is mistaken. The total energy E, and the mean dissipation ϵ, vary when the axial length L_x is modified. Both quantities diminish significantly when r_x increases from $r_x=1$ to $r_x \geq 2$. However, for larger aspect ratios $3 \geq r_x \geq 8$,

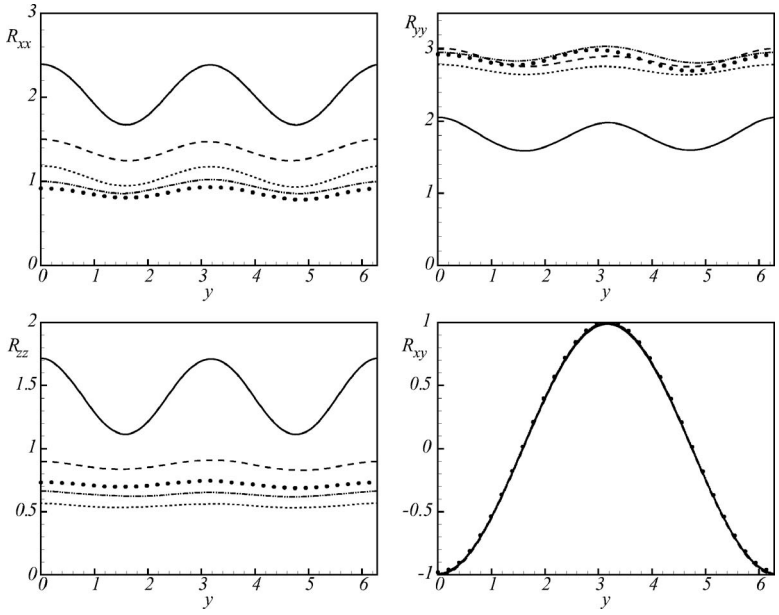

FIG. 3. Reynolds stresses averaged over t and z-x for different r_x with $r_y=r_z=1$: R_{xx} (top left), R_{yy} (top right), R_{zz} (bottom left), and R_{xy} (bottom right). The cases represented are: A01 ($r_x=1$, solid); A02 ($r_x=2$, dash); A04 ($r_x=4$, dot); A06 ($r_x=6$, chained-dot); and A08 ($r_x=8$, circle).

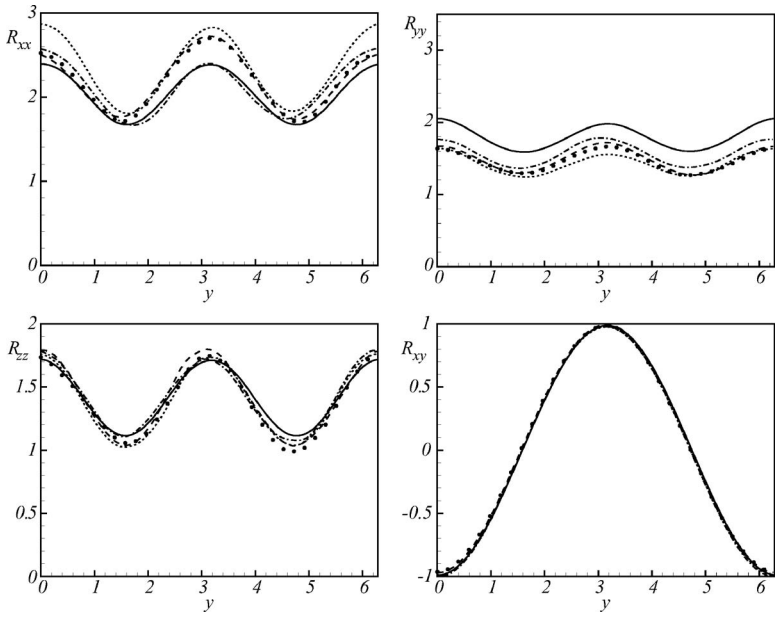

FIG. 4. Reynolds stresses averaged over t and z-x for different r_y with $r_x=r_z=1$: R_{xx} (top left), R_{yy} (top right), R_{zz} (bottom left), and R_{xy} (bottom right). A01 ($r_y=1$, solid); A01β ($r_y=2$, dash); A01γ ($r_y=3$, dot); A01δ ($r_y=4$, chained-dot); and A01ϵ ($r_y=6$, circle).

the energy remains almost constant and even slightly increases. This evolution indicates strong differences between the different cases for both the mean velocity field and the mean Reynolds stresses.

Since the forcing is along x and depends only on y, the problem is *a priori* independent of z. This relative insensitivity to r_z is confirmed by the results from cases A03a, A03b, and A03c. The global statistics are, however, also very much independent of r_y, as shown when comparing runs A01, A01β, A01γ, A01δ, and A01ϵ as well as runs A03a and A03β or A04 and A04β.

These properties are clearly illustrated in Fig. 2, where the mean longitudinal velocity component V_x is plotted for several runs. In all cases, the mean velocity is an almost perfect sine function, as expected from the forcing, but the amplitude decreases with increasing axial length (higher r_x). The results for run A01 are quite different from those obtained for the runs with a longer axial length. This behavior has also been observed for other characteristics of the flow, and is explained in Sec.V. On the contrary, the mean velocity profiles are almost independent of the value of r_y and r_z. The other mean velocity components are zero for all cases when one considers averaging over time and z-x.

The dependence on the computational box sizes appears also in the mean Reynolds stresses but with different trends. The influence of r_x on nonzero components of R_{ij} (considering averaging over t and z-x) is shown in Fig. 3. The R_{xy} component follows the behavior of the mean axial velocity but with opposite trend and a lower amplitude since those terms are related by Eq. (16). Except for the cubic case (A01), the R_{zz} component is nearly identical in all cases: This is a further indication that the dependence on the computational box sizes affects the z component less than the x and y components. The other two nonzero components (R_{xx} and

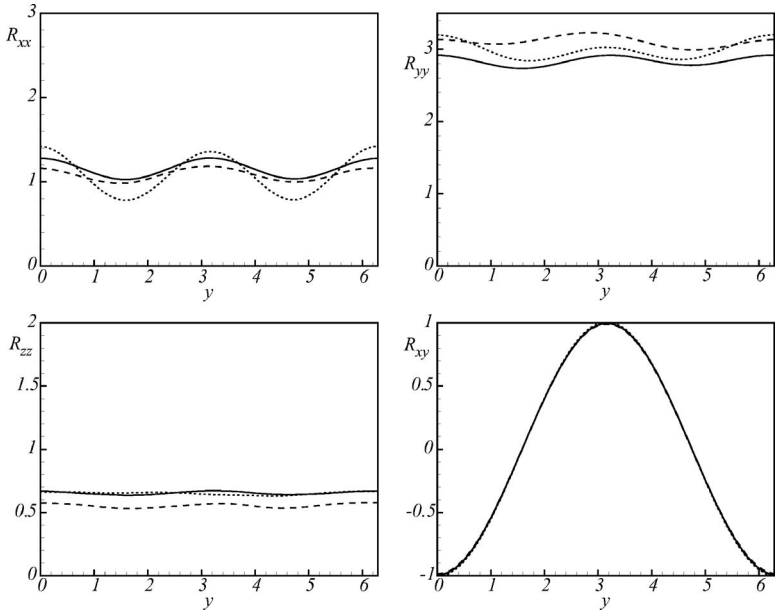

FIG. 5. Reynolds stresses averaged over t and z-x for different r_z with $r_x=3$ and $r_y=1$: R_{xx} (top left), R_{yy} (top right), R_{zz} (bottom left), and R_{xy} (bottom right). The cases represented are: A03a ($r_z=1$, solid); A03b ($r_z=2$, dash); and A03c ($r_z=3$, dot).

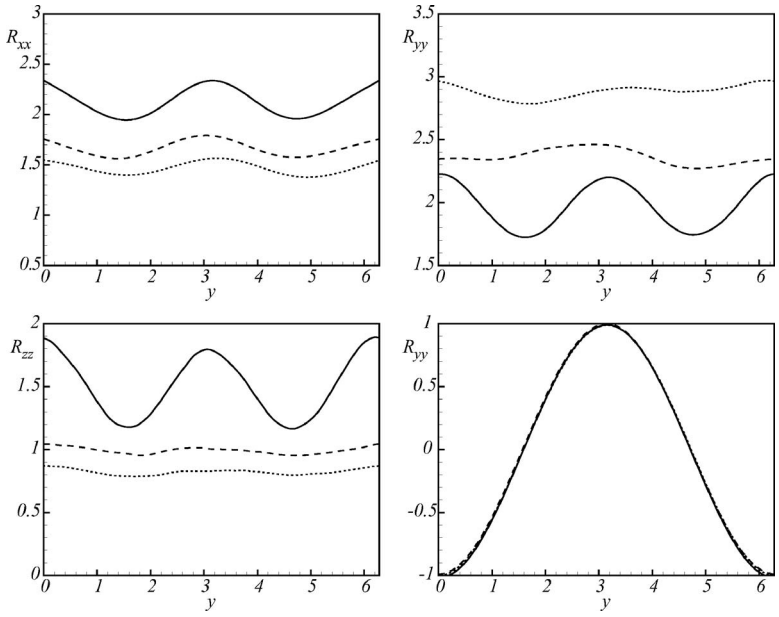

FIG. 6. Reynolds stresses averaged over t and z-x for different r_x with $r_y=r_z=1$: R_{xx} (top left), R_{yy} (top right), R_{zz} (bottom left), and R_{xy} (bottom right). The cases represented are: B01 ($r_x=1$, solid); B02 ($r_x=2$, dash); and B04 ($r_x=4$, dot).

R_{yy}) vary more with the longitudinal length, and strong deviations for the A01 case are observed again (see Sec. V). In all cases, the relatively small differences between the results for the cases A06 and A08 seems to indicate that a sort of asymptotic limit has been reached, leading to a universal behavior for very elongated boxes. Results in Figs. 4 and 5 show a much weaker dependence of the Reynolds stress components on the ratios r_y and r_z, confirming the observation made for the mean velocity in Fig. 2.

The evidence of dependence on the computational box sizes is observed for both series A and B (see Fig. 6). There are, of course, differences related to the Reynolds number. Indeed, there is little hope to observe Reynolds number independent statistics at the fairly moderate values ($\mathrm{Re}\approx 65-180$) that are reported in this study. However, the same trends are observed in both sets of results.

V. BREAKING OF TRANSLATIONAL INVARIANCE

In the case of a laminar Kolmogorov flow, the velocity field has a simple pattern. The x component of the velocity varies with the y direction only and has a sine shape, while the y and z components are zero:

$$V_x = \frac{A}{\nu k_f^2}\sin(k_f y). \tag{27}$$

In the case of a turbulent Kolmogorov flow, if one examines the velocity averaged over t and z-x, one recovers the simple pattern of the laminar case. The amplitude of the axial velocity sine function is however somewhat smaller and varies with the longitudinal length as described in the previous section. When the flow is turbulent, the time averaged velocity could be function not only of y, but also of x and z, leading to a breaking of the translational invariance.[8] This dependence could also vary with the axial extent of the simulation. Figure 7 shows the influence of r_x on the transverse vorticity ω_z, based on the averaged velocity in t and z, for five cases corresponding to $r_y=r_z=1$: A01, A02, A03a, A04, and A06. For the first case (cubic box) there is no dependence in x. In the second case ($r_x=2$), the flow pattern has a slight x dependence. For all cases with $r_x\geq 3$, there is a strong dependence in both x and y, and the mean flow pattern is characterized by two strong vortices of opposite sign. They are separated by a half-period in both the x and y directions. Even for very elongated boxes, only two vortices remain after averaging over a very long time. In the transitory periods (not shown here), a succession of positive and negative vortices with different amplitudes is observed. However, for very long integration times only the two strongest vortices survive. In the case A01 (which corresponds to the case that is traditionally studied), the longitudinal length is too small to allow the

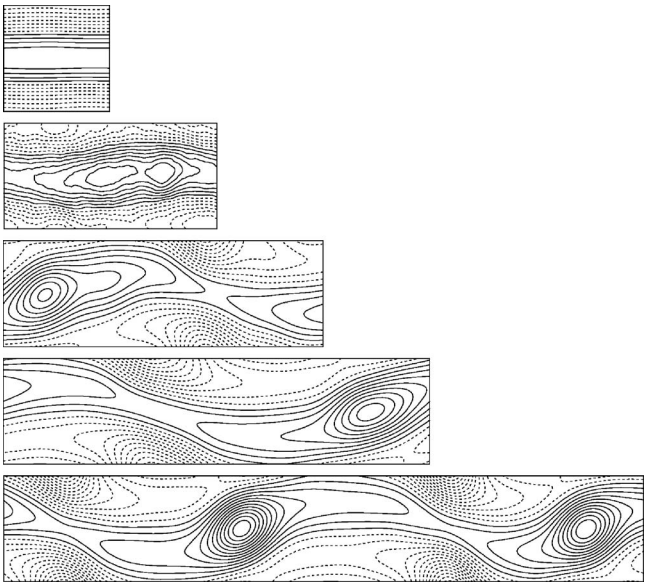

FIG. 7. Vorticity ω_z averaged over t and z, for $r_y=r_z=1$ and $r_x=1$, 2, 3, 4, and 6: A01, A02, A03a, A04, and A06 (from top to bottom). Positive vorticity and negative vorticity contours are shown using, respectively, solid and dashed curves. The vertical and horizontal directions are, respectively, y and x.

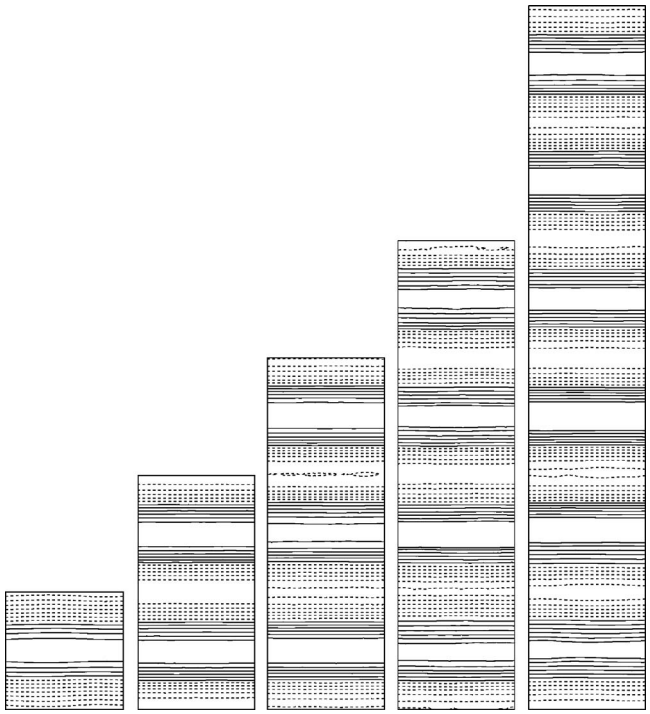

FIG. 8. Vorticity ω_z averaged over t and z, for $r_x=r_z=1$ and $r_y=1$, 2, 3, 4, and 6: A01, A01β, A01γ, A01δ, and A01ϵ (from left to right). Positive vorticity and negative vorticity contours are shown using respectively solid and dashed curves. The vertical and horizontal directions are, respectively, y and x.

appearance of two separate vortices. The flow characteristics are thus much different (and much simple) from those observed for the other cases. It should thus be acknowledged that the results obtained for the cubic geometry are rather "atypical" for the Kolmogorov flow and that the statistics of this flow depend strongly on r_x.

Figure 8 is similar to Fig. 7, but explores the influence of r_y on the transverse vorticity ω_z, based on the averaged velocity in t and z, for five cases corresponding to $r_x=r_z=1$: A01, A01β, A01γ, A01δ, and A01ϵ. The dependence on the ratio r_y appears to be very weak. These results are confirmed in Fig. 9 which shows the influence of r_y on the transverse vorticity ω_z for $r_x=3$ and $r_z=1$: A03a ($r_z=1$) and A03β ($r_y=2$). The structures appears to be almost independent of r_y and the observed patterns of the cases A03a and A03β differ only through the phases.

Obviously, the structures of ω_z, showed in Figs. 7 and 9 for $r_x>1$ have a typical length scale larger than the forcing

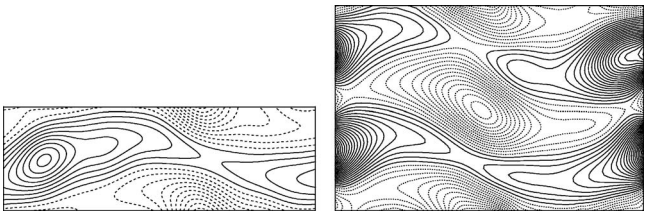

FIG. 9. Vorticity ω_z averaged over t and z, for $r_y=1$ and 2 (respectively, cases A03a and A03β). The structures are very similar and appear to be repeated twice in the $r_y=2$ case, without a major difference.

length. In that sense, it could be interpreted as a possible inverse energy cascade mechanism, as discussed by Borue and Orszag[8] and Sulem *et al.*[14] for the Kolmogorov flow. It is, however, quite different from two-dimensional turbulence inverse energy cascades, since it only feeds the mode with $k_x/k_f<1$, while modes $k_z/k_f<1$ and $k_y/k_f<1$ are not excited. Even though this does not really give a full explanation of the observed phenomena, it might be reasonable to describe our numerical results by referring to them as an "anisotropic inverse cascade." Another difference between more traditional inverse energy cascades observed in two-dimensional, or quasi-two-dimensional turbulence, and our observations is also made clear when considering the results of Smith *et al.*[15] Indeed, these authors used, among other diagnostics, the ratio between the energy injection rate and the energy dissipation rate to characterize the transition between the two-dimensional inverse cascade and the three-dimensional direct cascade. In the three-dimensional direct cascade, this ratio is close to 1. In the two-dimensional inverse cascade, this ratio is smaller than 1. In our simulations, this ratio is always close to 1 (which is equivalent to have $\gamma_2=0$.)

The vortices shown in Figs. 7 and 9 yield a strong velocity, as illustrated in Fig. 10. Except for small longitudinal lengths (A01 and A02), the amplitude of the y component of the velocity averaged in time and y-z, $\langle u_y\rangle_{t,y\text{-}z}$, is nearly constant and larger than the amplitude of $\langle u_x\rangle_{t,y\text{-}z}$. Thus, despite the fact that the forcing is in the x direction, the mean flow is mainly perpendicular to it, as illustrated in Fig. 11 for the cases A03a and A03β. We also note that the axial phase of the flow is randomly determined by the initial conditions. The amplitude of $\langle u_z\rangle_{t,y-z}$ (not shown here), is in all cases much smaller than the amplitude of $\langle u_x\rangle_{t,y-z}$ and $\langle u_y\rangle_{t,y-z}$.

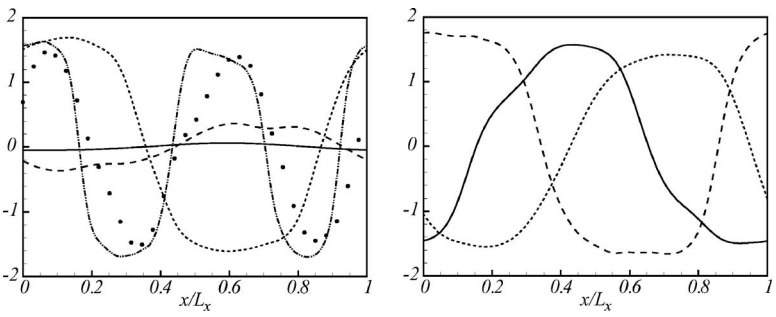

FIG. 10. The y component of the velocity averaged in time and y-z, $\langle u_y\rangle_{t,y\text{-}z}$. Left - various cases with different axial lengths: A01 (solid); A02 (dash); A04 (dot); A06 (chained-dot); A08 (solid circle). Right - cases with different transversal lengths: A03a (solid); A03b (dash); A03c (dot).

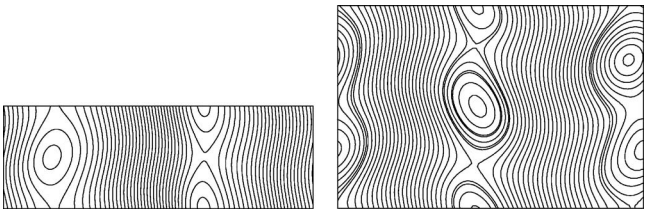

FIG. 11. Mean streamlines for the cases A03a and A03β.

VI. DISCUSSION

The DNS presented here clearly show that the Kolmogorov flow exhibits statistical properties that depend on the computational boxes sizes. The main effect of the computational box in the spectral code used here is to impose the periodicity length on the velocity through periodic boundary conditions. Consequently, the turbulence statistics in the Kolmogorov flow strongly depend on the boundary conditions that have been chosen. Furthermore, it has been observed that some symmetries compatible with both the boundary condition and the forcing are broken in the statistical sense. In particular, the translational invariance (the independence of x for both the forcing and the domain) is observed to be broken at the statistical level, for the time averaged solution of the Navier-Stokes equation.

These properties—box-size dependence and breaking of the translational invariance—make the Kolmogorov flow a very rich and complex test case. Being easily computed with a spectral code, the Kolmogorov flow could thus be considered as an appropriate test case for assessing large-eddy simulation of inhomogeneous, anisotropic, and sheared turbulent flow, without having to deal with the problem of wall modeling.

ACKNOWLEDGMENTS

This work has been supported by the Fonds National pour la Recherche Scientifique (Belgium, FRFC 2.4542.05), the Fonds Defay, the Communauté Française de Belgique (ARC 02/07-283) and the contract of association EURATOM Belgian state. The content of the publication is the sole responsibility of the authors and it does not necessarily represent the views of the Commission or its services.

[1] A. L. Frenkel, "Stability of an oscillating Kolmogorov flow," Phys. Fluids A **3**, 1718 (1991).
[2] A. Thess, "Instabilities in two-dimensional spatially periodic flows. Part 1: Kolmogorov flow," Phys. Fluids A **4**, 1385 (1992).
[3] Z. S. She, "Metastability and vortex painting in the Kolmogorov flow," Phys. Lett. A **124**, 161 (1987).
[4] D. Armbruster, R. Heiland, E. J. Kostelich, and B. Nicolaenko, "Phase space analysis of bursting behaviour in Kolmogorov flow," Physica D **58**, 392 (1992).
[5] I. Bena, M. M. Mansour, and F. Baras, "Hydrodynamic fluctuations in the Kolmogorov flow: Linear regime," Phys. Rev. E **59**, 5503 (1999).
[6] I. Bena, F. Baras, and M. M. Mansour, "Hydrodynamic fluctuations in the Kolmogorov flow: Nonlinear regime," Phys. Rev. E **62**, 6560 (2000).
[7] G. Boffetta, A. Celani, and A. Mazzino, "Drag reduction in the turbulent Kolmogorov flow," Phys. Rev. E **71**, 036307 (2005).
[8] V. Borue and S. A. Orszag, "Numerical study of three-dimensional Kolmogorov flow at high Reynolds numbers," J. Fluid Mech. **306**, 293 (1996).
[9] S. L. Woodruff, J. M. Seiner, and M. Y. Hussaini, "Grid-size dependence in the large-eddy simulation of Kolmogorov flow," AIAA J. **38**, 600 (2000).
[10] S. L. Woodruff, J. V. Shebalin, and M. Y. Hussaini, "Large-eddy simulations of a non-equilibrium turbulent Kolmogorov flow," 49th Annual Meeting of the DFDMP, Syracuse, NY, Nov. 24–26, 1996.
[11] R. S. Rogallo, "Numerical experiments in homogeneous turbulence," NASA TM-81315 1981.
[12] S. Childress, R. R. Kerswell, and A. D. Gilbert, "Bounds on dissipation for Navier-Stokes flow with Kolmogorov forcing," Physica D **158**, 105 (2001).
[13] J. V. Shebalin and S. L. Woodruff, "Kolmogorov flow in three dimensions," Phys. Fluids **9**, 164 (1997).
[14] P. L. Sulem, Z. S. She, H. Scholl, and U. Frisch, "Generation of large-scale structures in three-dimensional flows lacking parity invariance," J. Fluid Mech. **205**, 341 (1989).
[15] L. M. Smith, J. R. Chasnov, and F. Waleffe, "Crossover from two- to three-dimensional turbulence," Phys. Rev. Lett. **77**, 2467 (1996).